Harmonic Elimination and dc–link Voltage Balancing in Bipolar Hybrid Microgrid by ILCs: A Review

Harmonic Elimination and dc–link Voltage Balancing in Bipolar Hybrid Microgrid by ILCs: A Review

S Vasantharaj[1*], V Indra Gandhi[2]

[1]Research Scholar, Vellore Institute of Technology, Vellore
[2]Associate Professor, Vellore Institute of Technology, Vellore
[*]Corresponding author E-mail: Vasantharaj.s@vit.ac.in

Abstract: In this advanced power system scenario, the bipolar hybrid microgrid application plays a vital role, which owns both DC and AC bus instantaneously. In this grid-connected technology, renewable energy performs a major role in the generation of power demand. Due to the alternating nature of renewable sources, the grid should have stability with different energy sources like battery storage systems, vehicle to grid, etc. Hence, to retain the quality of power supply it is more significant to consider an interlinking bidirectional converter between a source and the grid. The most important indispensable component in the bidirectional link is an AC/DC bidirectional converter. This paper elaborates about the advantages and disadvantages of the prevailing AC/DC bidirectional converter topologies for the advancement in the microgrid applications. These types of three-phase ac/dc bidirectional converters are preferred to reduce the THD content in the grid side, power factor correction, and regulated dc output voltage with unidirectional and bidirectional power flow. The dc-link voltage has balanced at the dc bus with these bidirectional topologies. By use of this bidirectional converter, it has designed to perform various essential applications in the microgrid with the help of space vector modulation.

KEYWORDS:
Bipolar Hybrid microgrid, interlinking converter, THD, Space vector Modulation, Voltage Balancing, Converter, Hysteresis comparator.

Nomenclature:

C	dc-link capacitor	V_{ref}	Reference Output Voltage
CSI	Current Source Inverter	V_a	Line to neutral Voltage
EMI	Electromagnetic Interference	I_a	Line Current
BHM	Bipolar Hybrid Microgrid	V_{dcl}	DC-link Voltage
WLAN	Wireless Local Area Network	U_{ref}	Normalized Voltage Vector
SVM	Space Vector Modulation	MPPT	Maximum Power Point Tracking
ESS	Energy Storage System	BW	Bandwidth
IoT	Internet of Things	PV	Photovoltaic
DG	Distributed Generation	MG	Microgrid

Introduction:

Smart grid plays a pivotal role in this upcoming power system era by the use of computer-based remote control and automation [1–7]. This smart grid performs with two-way power flow and information flow with digital communication techniques and computer processing. During the initial state, it is used in electrical networks, from the windmills and power plants to distribute power to consumers of electricity in homes and businesses. The distributed MG [8–15], contains DG units, ESS, and distributed loads that utilize isolated mode or grid-connected mode. The VSI is a frequently used power electronic converter that connects between DGs and the grid. The Distributed generator injects active and reactive power [15–19], to control this active and reactive power interlinking inverter regulates the phase angle and the magnitude of the output voltage. By the use of appropriate control methods, this inverter compensates more power quality issues like voltage and current harmonics. In [20], it is proposed that the lower order harmonics can be eliminated by the use of proper SVM technique in the interlinking converter that is used between DGs and the grid. Similarly, in [21], it is proposed that the microgrid controls the

frequency domain operation. The basic principle of this bidirectional converter is to convert direct current to alternating current and vice versa. Different applications weights distinct features and hence different types of bidirectional converters are proposed for each of its applications. For example, vehicle charger desires to be dense and fewer heaviness, while the bidirectional linkage of PV generation distress about the permanence and the reliability of its performance.

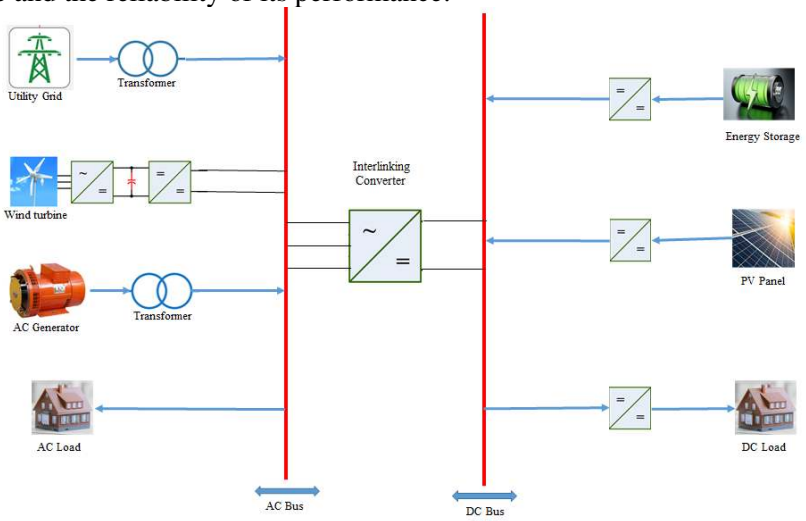

Figure 1. Diagrammatic Representation of Interlinking Converter for Bipolar Hybrid microgrid.

The bipolar hybrid microgrid with a bidirectional converter is shown in Fig. 1. Hence, different types of converter topologies are used which results in different levels of excellence and difficulty. Furthermore, the suitable bidirectional converter topology is selected for the requirement of the application. Fig. 2 shows the different methods of bidirectional converter. By use of a different type of control, methods like Particle Swarm Optimization and hysteresis current controllers are used for the elimination of lower order harmonics. In the same way, the load will be compensated by the use of droop controller in the microgrids. To eliminate the resonance under harmonic frequencies, to control active and reactive powers, improve system unbalance, balancing of V_{dcl}, and to limit the harmonic voltage and current these types of compensators are used. The voltage and current harmonics are compensated by the use of one proposed converter for the microgrid [22], which contains one distributed generator with two inverters. In these two inverters, first one is operated to compensate voltage harmonics in the load side and another inverter is used to compensate the current harmonics. Similarly, the THD of injected current, voltage through ILC, V_{dcl}, and dc voltage ripple will be evaluated.

In [23], to improve the stability of harmonic current and to reduce reactive power sharing, the output of the reference voltage of each distributed generator is injected with high-frequency harmonic voltage. By varying the BW of the control loop, it is applicable to have accurate power sharing by modifying the output impedance of individual inverter under closed loop condition. It is proposed to develop nonlinear load sharing and increase in voltage control gain with the help of improvement in distortion power (D) which is shared by the DGs. This method is used to reduce the voltage control stability.

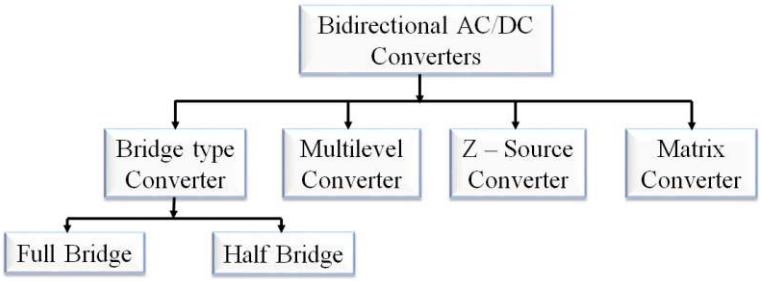

Figure 2. Different methods of the bidirectional converter.

In [24], improvement in harmonic current sharing is obtained by harmonic virtual impedance schemes. By varying the V_{ref} of the DG by the use of load current feed forward loop virtual harmonic impedance is varied. Moreover, for the difficulties associated with imbalanced power sharing in isolated microgrids a categorized control structure having more control loops has been proposed in [25].
The survey taken for balancing the dc-link poles and the same is evaluated for dc-link balancing strategies with the help of this different bidirectional converter [26–27]. The main features of this each bidirectional converter elaborated in Section 2 and explain about the elimination method for lower order harmonics with the analyses of a common mechanism for a grid-tied ILC. In section 3, carrier-based modulation and its associated V_{dcl} balancing strategies elaborated through full-scale voltage balancing competence with the different types of SVM methods. In section 4, it deals with the future scope and IoT based renewable energy sources.

2. Types of interlinking converters:

The different types of interlinking converters used in the bipolar hybrid microgrids are explained as follows,

2.1. 10 – Switch Interlinking Converter:

Fig. 3 shows the circuit diagram for 10-switch converter. An ac output voltage of 2/3 level with three-wire bipolar dc topology is proposed by 10 switch converter. The conventional voltage source converter (VSC) added with S1A to S4A switches to obtain this proposed converter. This converter comprises of 3 main legs and an auxiliary leg contains 4 switches having three different forms of switching states (P, O, N). The switching states and their illustration are shown in table 1.

Table 1. Switching states of Interlinking converter.

Switching State	ON switches		Terminal voltage
P	S1A	S1 or S3 or S5	E
O	S2A S3A	S1 or S3 or S5 S2 or S4 or S6	0
N	S4A	S2 or S4 or S6	-E

The auxiliary leg of switches S2A or S3A produces a switching state O and these switches depend on former leg states. The remaining switching states are said to be understandable. Eight and twenty-seven switching vectors of two-level and three-level VSI is compared with the 10–switch converter, which has twenty-one switching vectors that contain eighteen active, and three zero vectors (PPP, OOO, NNN). The twenty-one switching vectors of 10-switch converter are split as three zero vectors, which are sited midpoint of a hexagon including six large and twelve small vectors. The dc-link poles are short-circuited due to this 10-switch converter by having this medium level vectors.
The 10-switch converter is suitable for high power applications because it contains both the advantages of 2-level and 3-level converter simultaneously. In [26], it explains about the combined topology of three-level neutral point clamped (NPC) and two level VSC. This gives the advantages of 3-level converter. 10-switch converter yields a composite of two and three-level AC voltage.

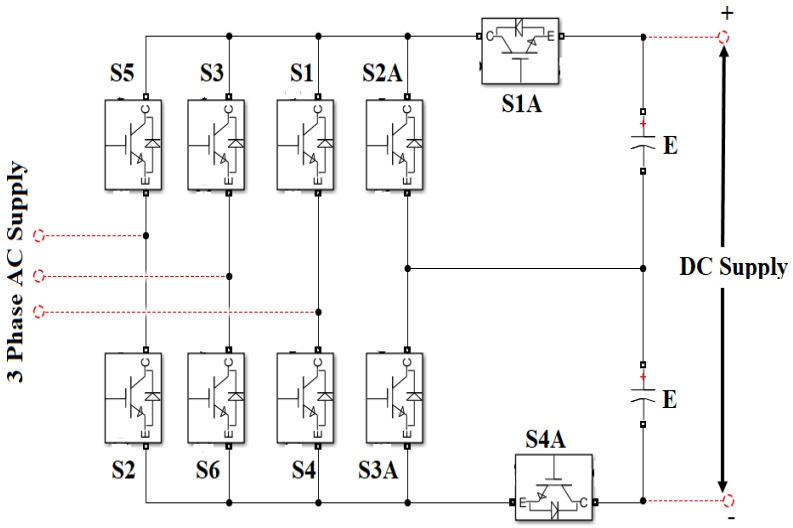

Figure 3. Circuit Diagram for 10 switch AC/DC interlinking converter.

2.2. Full Bridge bidirectional Converter:

2.2.1. System description

In [22-26], the converter dynamic response was verified by various circumstances like the difference in a voltage source, the difference in load and variations in both load, and voltage source. Fig. 4 shows a three-phase AC/DC bidirectional converter, in which the grid is coupled with the AC side of the converter and for DC side; is coupled to DC loads. The resistor with a toggle switch is used to test the variation in load. The full-bridge bidirectional converter switches perform three types of operating modes namely, rectification, inversion, and Shut-Down Modes.

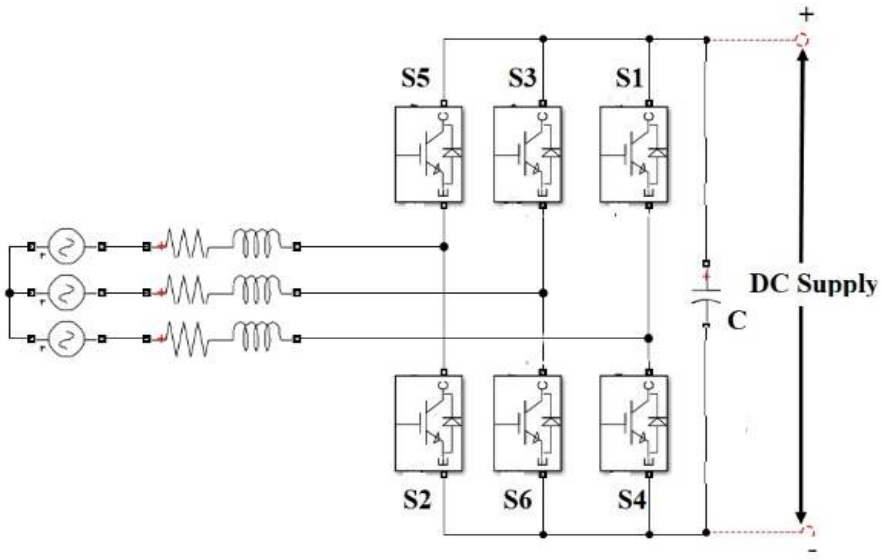

Figure 4. Circuit diagram for full-bridge AC/DC bidirectional converter.

2.2.2. Inversion mode

By this inversion mode, the bidirectional converter operates under the unity power factor (UPF) because of reactive power in the utility grid is maintained to zero. By increasing the DC source which is above the DC load then the converter can function in adjustable reactive power to change the power factor. Hence the power is transferred from dc side to ac side. The inversion mode is justified by the phase

difference of 180^0 between the line to neutral voltage V_a and the line current i_a by having proper sinusoidal waveform with low THD.

2.2.3. Shut-Down Mode

If the power delivered or absorbed by the grid is equal then this is said to be Shut-Down Mode (S-DM). At this instant, the converter is in the shutdown state. By attaining this delivered and observed power to equal, it is achieved by varying the load until it becomes to shut down mode.

2.2.4. Rectification mode

If the voltage of DC load is more than the voltage of DC source then the converter attains rectification mode (RM). By increasing the grid side voltage, rectification mode is achieved. Hence, the dc-bus voltage V_{dc} drops relative to its reference value V_{dcr}. The bidirectional converter is used to inject the power from the AC grid to the DC load side.

2.3. Bidirectional Matrix Converter

Matrix converter is one of the best exciting families in the converter. By the use of matrix converter, ac-ac power conversion is achieved without any intermediate energy storage elements. Fig. 5 shows the topology of the High Frequency Link Matrix Converter (HFLMC). Each bidirectional switch S_{xy} is self-possessed of 2 transistors S_{xy1} and S_{xy2} (x = a, b, c and y = P, N) in a mutual source structure, demands single fluctuating source. In this topology, a matrix converter operates as a CSI and supplies voltage to the high frequency transformer (HFT). Furthermore [29, 30], to shorten the description transformer is modeled has leakage inductance L on the primary side with an ideal transformer of turns ratio n. the P and N bar is connected with a single input phase which is fed by a voltage source of matrix converter shown in fig. 5.

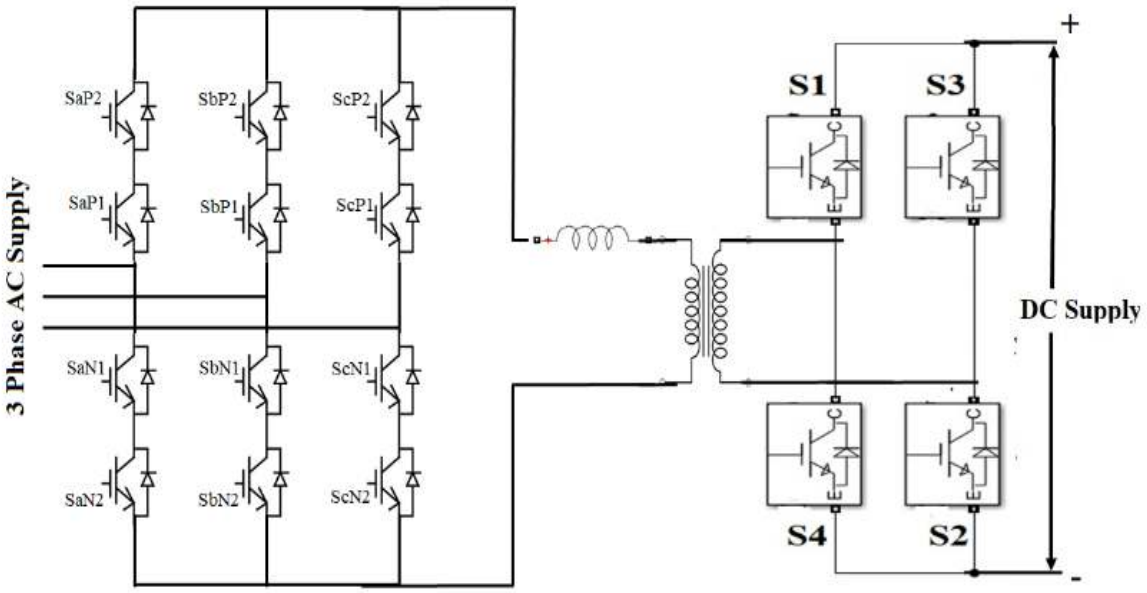

Figure 5. Circuit Diagram for AC/DC bidirectional matrix converter.

The bidirectional matrix converter performs the following advantages: 1) one-step power transformation 2) two way power transfer 3) galvanic separation 4) nonexistence of dc-link 5) voltage equivalent by the transformer turns ratio and 6) extended provision life. Same way the disadvantage of this converter is harmonic content, which is present in the current of matrix converter; an EMI filter is essential to eliminate these harmonics in the input current. Another disadvantage of this topology contains transformer having inductive nature, which allows a maximum amount of current flow in the circuit.

2.4. Dual Active Bidirectional Converter:

The major applications of Dual active bidirectional converter are renewable power generation; plug-in hybrid vehicles and supply systems because of high frequency isolation and controllability of active power flow in the distribution end. This proposed converter is used to operate all the operating modes like inversion and rectification mode of the converter that results in logical approximation of power transmission, rms current, and examination of soft-switching circumstances for power strategies.

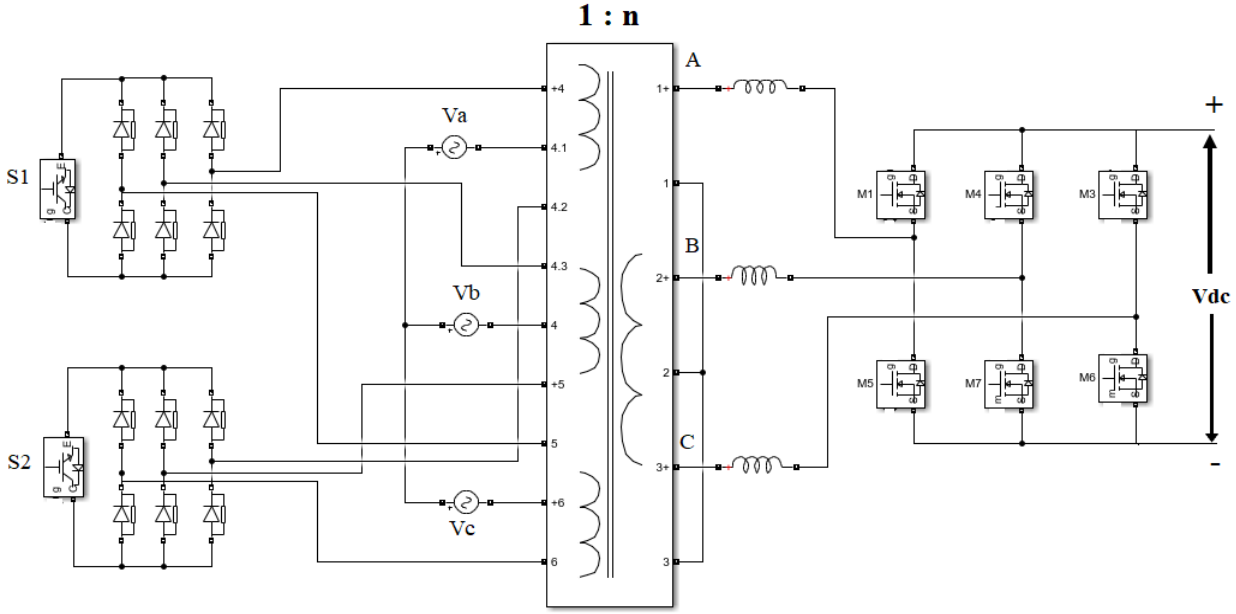

Figure 6. Circuit diagram for dual active AC/DC bidirectional converter.

Fig. 6 shows the three winding transformers for each phase with the turns ratio of 1 : n. the input phase voltages V_a, V_b and V_c are commonly connected to the two primary windings of the transformer. Three input phases V_a, V_b and V_c are connected to a common terminal of 2 primary windings of the transformer. The primary side of the three winding transformer comprises of two three-phase diode bridge in a push-pull configuration with two active switches S_1 and S_2. The inductance L that is present on the secondary side of the transformer signifies the total leakage inductance of the transformer ($L = n2L_p + L_s$). The primary and secondary winding needs external inductance that is to be connected in series in the case of the inductor L is considered more than the leakage inductance. The two level voltage source inverter (VSI) is connected on the secondary side of the transformer. Then the VSI is connected to the dc source. The phase voltage equation of the primary side is given in equation (1) with a frequency of $\omega = 2\pi f = 2\pi/T$ and amplitude V_{grid}. The primary-side switches S_1 and S_2 are switched in a complementary method with a 50% duty ratio at a frequency $f_s = 1/T_s$, such that $f_s >> f$. Accordingly, the secondary-side has high frequency square wave with line frequency which is shown in equation (2).

$$V_a = V_{grid} \sin(2\pi f t) \quad (1)$$

$$V_{AN} = \pm nV_a = \pm nV_{grid} \sin(2\pi f t) \quad (2)$$

(+ with S_1 ON, − with S_2 ON).

The advantages of this bidirectional converter are one-step transformation, no unpredictable halfway dc-link capacitor, less number of switches, modest control scheme, open-loop UPF operation, bidirectional power flow, and partial soft switching.

The comparative analysis of different types of ac/dc bidirectional converter has shown in table 2.

Table 2. Comparative analysis for AC/DC bidirectional Converters.

	Voltage source Converter	**Multi-level converter**	**Matrix converter**	**10 switch converter**
Types	i) Half bridge ii) Full bridge	i) Diode Clamped. ii) Flying Capacitor iii) Cascaded H – Bridge	i) Direct ii) In-direct	N/A
Switches	6	16	20	10
Capacitor	1 filter capacitor of dc side	No need	No need	2 filter capacitor of dc side
Inductor	No need	Filter inductor on ac side	Filter inductor on ac side	No need
Transformer	N/A	1	1 : n	N/A
Components Required	Less	More	More	Less
Controller Circuit	Complex	Complex	Simple	Simple
Harmonic Content	High	Less	Less	Less
Filter Circuit	High	Small	Small	Small
Voltage Stress	Low	Low		Low
DC Voltage Control	Needs additional circuit to boost rectified dc output.	Needs additional circuit to control the voltage to match desired ac output voltage with grid.	No need.	No need.
Application	Operates at low power application.	Operates in high voltage and high power applications.	Used in medium voltage application.	Used in high voltage application.
Switching Loss	High	Moderate	Low	Low
Efficiency of a converter	Less	Medium	More	More

3. Classification of Different SVM Methods:

3.1. Type I:

A dc-link voltage balancing capability is presented in this subdivision by the use of proposed SVM technique. The foremost objective of this novel SVM method is to improve dc-link voltage and decreases output of current THD and common mode voltage. Similarly, this proposed SVM does not need any passive or active elements. The SVM, consists of six sectors and these sectors are subdivided into small parts having the shapes of trapezoid and triangle. By using this SVM there will be an increase in current THD, switching configuration and neutral point voltage deviation. SVM used is operated under both balanced and unbalanced conditions which lead to a decrease in extra converter costs, volume and power loss.

3.1.1. Region determination

Initially, the corresponding SVM for three level VSI, the V_{ref} is induced to measure its angle and amplitude. Then, it is to be determined that were V_{ref} is located and to identify the sector and region for this reference voltage vector. Each sector region is similar to one another and it is validated in fig. 7. The region and the sector in which it is located will be stipulated by the angle and amplitude of the V_{ref}.

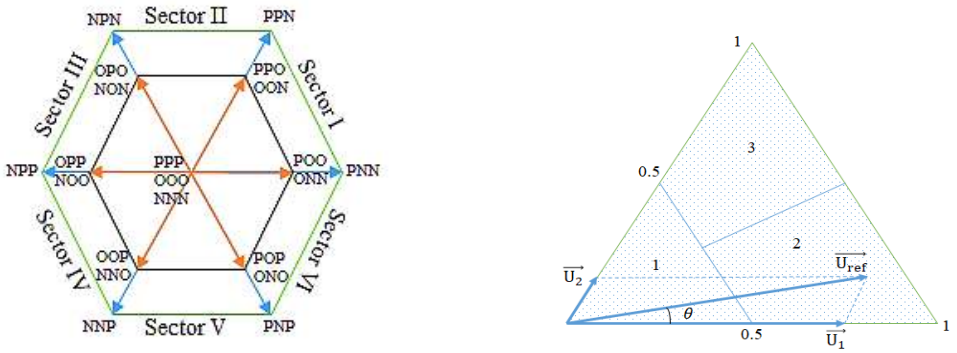

Figure 7. SVM for 10 switch converter and its sector representation for normalized voltage vector

The normalized reference voltage vector (U_{ref}) is attained to compute and locate the section of V_{ref} for the interlinking converter. The vectors U_1 and U_2 obtain the resultant vector of U_{ref} which is shown in equation (3), (4) and table 3.

$$U_1 = U_{ref}\left(Cos\theta - \frac{sin\theta}{\sqrt{3}}\right) \tag{3}$$

$$U_2 = 2U_{ref}\left(\frac{sin\theta}{\sqrt{3}}\right) \tag{4}$$

To eliminate over modulation these calculations are used. The U_{ref} angle and its amplitude are used to change the region of respective sectors with the values U_1 and U_2 maximum of 1. The U_{ref} amplitude goes in the trapezoidal area, which contains two equal areas after passing the region 1 area, which is shown in fig 7. The trapezoidal region changes from 2 to 3 when the reference voltage vector attains 30^0 which is equal to $\sqrt{3}/2$. The non-existence of medium voltage is reimbursing with the split up trapezoidal regions of 2 and 3.

Table 3. Region identification based on $U_{ref.}$

Case	Angle (θ)	Region
$U_1 \leq 0.5$ and $U_2 \leq 0.5$ & $U_1+U_2 \leq 0.5$	NA	1
$U_1 > 0.5$ or $U_2 > 0.5$ or	$\theta \leq 30^0$	2
$U_1 + U_2 > 0.5$	$\theta > 30^0$	3

3.1.2. Symmetrical switching sequence

This type of switching sequence is organized to minimize the THD, which is considered as the main objective of this proposed method.

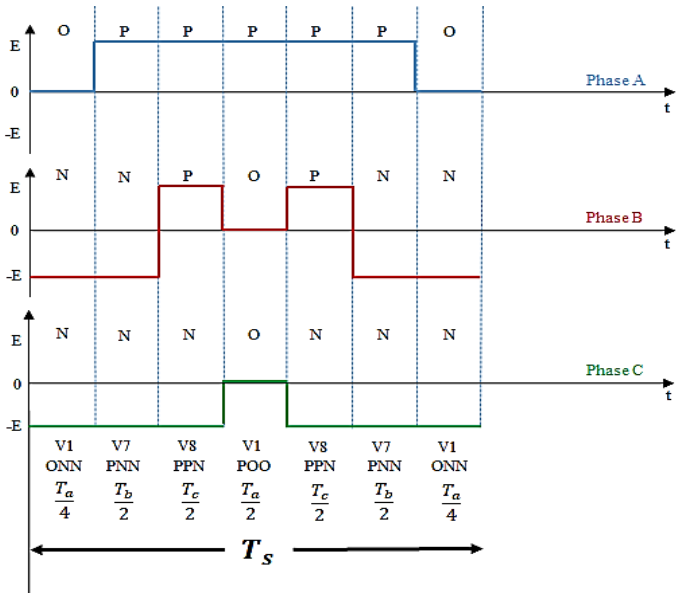

Figure 8. Switching Sequence of Sector 1.

The switching time (T_s) for sector 1 with switching sequence is shown in Fig. 8. Since fig. 7 shows identical sectors and regions, hence by having the reference of the first sector, the vector selection and switching sequence of this proposed SVM for all the six sectors eighteen regions are calculated.

3.2 Type II:

3.2.1. Sector Partition:

Table 4 shows the relation between switching stages and voltage vectors of the SVM. In this type of SVM $i_a > 0$, $i_b < 0$, $i_c < 0$, and $i_a > 0$, $i_b > 0$, $i_c < 0$ considered as an example for the rectification mode of the converter. Fig. 9 consists of six non-zero vectors, hence the SVM is divided into six sectors. The traditional partition of the SVM has six sectors that are shown in full lines and the scattered lines additionally split the sectors into 12 rendering to the direction of three-phase ac current flow.

Table 4. Voltage vectors verses Switching States

$i_a > 0, i_b < 0, i_c < 0$							$i_a > 0, i_b > 0, i_c < 0$						
S_a	**S_b**	**S_c**	**S_d**	**S_e**	**Sign {vT}**	**V**	**S_a**	**S_b**	**S_c**	**S_d**	**S_e**	**Sign {vT}**	**V**
0	0	0	1	1	0	0	0	0	0	1	1	0	0
0	0	1^+	1	1	0	0	0	0	1^+	1	0	-	$-\alpha^2\frac{2}{3}\frac{n_p}{n_s}v_{dc}$
0	1^+	0	1	1	-	0	0	1^-	0	1	1	0	0
0	1^+	1^+	1	0	+	$\frac{2}{3}\frac{n_p}{n_s}v_{dc}$	0	1^-	1^+	1	0	-	$\frac{2}{3}\frac{n_p}{n_s}v_{dc}$
1^-	0	0	0	1	+	$\frac{2}{3}\frac{n_p}{n_s}v_{dc}$	1^-	0	0	1	1	0	0
1^-	0	1^+	0	1	+	$-\alpha\frac{2}{3}\frac{n_p}{n_s}v_{dc}$	1^-	0	1^+	1	0	-	$\alpha\frac{2}{3}\frac{n_p}{n_s}v_{dc}$
1^-	1^+	0	0	1	+	$-\alpha^2\frac{2}{3}\frac{n_p}{n_s}v_{dc}$	1^-	1^-	0	0	1	+	$-\alpha^2\frac{2}{3}\frac{n_p}{n_s}v_{dc}$
1^-	1^+	1^+	1	1	0	0	1^-	1^-	1^+	1	1	0	0

The 12 sectors are numbered according to the value of three-phase voltage v_α and v_β in stationary two phase Coordinates. Hence, the six sets of intermediate variables are given below:

$$v_{ref1} = v_\beta \tag{5}$$

$$v_{ref2} = v_\alpha \tag{6}$$

$$v_{ref3} = \frac{1}{2}\left(\sqrt{3}v_\alpha - v_\beta\right) \tag{7}$$

$$v_{ref4} = \frac{1}{2}\left(v_\alpha - \sqrt{3}v_\beta\right) \tag{8}$$

$$v_{ref5} = -\frac{1}{2}\left(\sqrt{3}v_\alpha - v_\beta\right) \tag{9}$$

$$v_{ref6} = \frac{1}{2}\left(-v_\alpha - \sqrt{3}v_\beta\right) \tag{10}$$

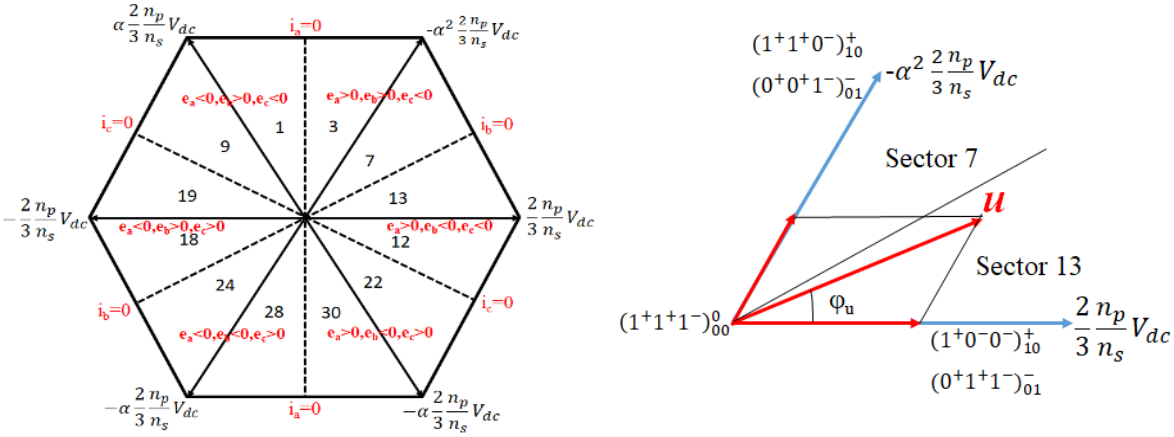

Figure 9. Sector Partition and Inverter mode of Sector 13 and 7.

If $v_{ref1} > 0$, A = 1; otherwise, A = 0. If $v_{ref2} > 0$, B = 1; otherwise, B = 0. If $v_{ref3} > 0$, C = 1; otherwise, C = 0. If $v_{ref4} > 0$,D = 1; otherwise, D = 0. If $v_{ref5} > 0$, E = 1; otherwise, E = 0. If $v_{ref6} > 0$, F = 1; otherwise, F = 0. The sector number is defined by N = A + 2B + 4C + 6D + 8E + 10F. Fig. 9 shows h sector partition and inverter mode of sector 13 and 7.

3.2.2. Vector Synthesis Method

By obeying the following laws, we can obtain the vector synthesis method: 1) retain the transformers voltage–second balancing; 2) decrease in switching loss; and 3) decrease in conduction loss.

3.2.3. Inverter Mode:

The three-phase inverter has two non-zero vectors in two different directions to produce the targeted vector with the use of SVM algorithm which is shown in sector 13 ($i_a < 0$, $i_b > 0$, $i_c > 0$). However, transformers voltage – second balancing is not guaranteed. Hence, it is considered three nonzero vectors with the sequence of switching-state are given in equation 11:

$$(1^+0^-0^-)^+_{10} \rightarrow (1^+1^-0^-)^+_{10} \rightarrow (1^+1^-1^-)^0_{00} \rightarrow (0^+1^-1^-)^-_{01} \Big| t = \frac{T_s}{2}$$

$$\rightarrow (0^+1^-1^-)^-_{01} \rightarrow (1^+1^-1^-)^0_{00} \rightarrow (1^+1^-0^-)^+_{10} \rightarrow (1^+0^-0^-)^+_{10} \Big| t = T_s \tag{11}$$

In sector 7 ($_ia < 0$, $i_b < 0$, $i_c > 0$), the sequence of switching-state are given in equation 12:

$$(0^+0^+1^-)^-_{01} \rightarrow (0^+1^+1^-)^-_{01} \rightarrow (1^+1^+1^-)^0_{00} \rightarrow (1^+1^+0^-)^+_{10} \Big| t = \frac{T_s}{2}$$

$$\rightarrow (1^{+}1^{+}0^{-})^{+}_{10} \rightarrow (1^{+}1^{+}1^{-})^{0}_{00} \rightarrow (0^{+}1^{+}1^{-})^{-}_{01} \rightarrow (0^{+}0^{+}1^{-})^{-}_{01} \Big| t = T_s \quad (12)$$

Fig. 10 shows the inverter mode operation of driving signals in sectors 13 and 7.

3.2.4. Rectifier Mode:
In sector 13 ($i_a > 0$, $i_b < 0$, $i_c < 0$), the sequence of switching-state are given in equation 13:

$$(1^{-}00)^{+}_{01} \rightarrow (1^{-}1^{+}0)^{+}_{01} \rightarrow (1^{-}1^{+}1^{+})^{0}_{11} \rightarrow (01^{+}1^{+})^{-}_{10} \Big| t = \frac{T_s}{2}$$
$$\rightarrow (01^{+}1^{+})^{-}_{10} \rightarrow (1^{-}1^{+}1^{+})^{0}_{11} \rightarrow (1^{-}1^{+}0)^{+}_{01} \rightarrow (1^{-}00)^{+}_{01} \Big| t = T_s \quad (13)$$

In sector 7 ($i_a > 0$, $i_b > 0$, $i_c < 0$), the sequence of switching-state are given in equation 14:

$$(001^{+})^{-}_{10} \rightarrow (01^{-}1^{+})^{-}_{10} \rightarrow (1^{-}1^{-}1^{+})^{0}_{11} \rightarrow (1^{-}1^{-}0)^{+}_{01} \Big| t = \frac{T_s}{2}$$
$$\rightarrow (1^{-}1^{-}0)^{+}_{01} \rightarrow (1^{-}1^{-}1^{+})^{0}_{11} \rightarrow (01^{-}1^{+})^{-}_{10} \rightarrow (001^{+})^{-}_{10} \Big| t = T_s \quad (14)$$

The driving signals in sectors 13 and 7 under rectifier mode are shown in Fig. 10.

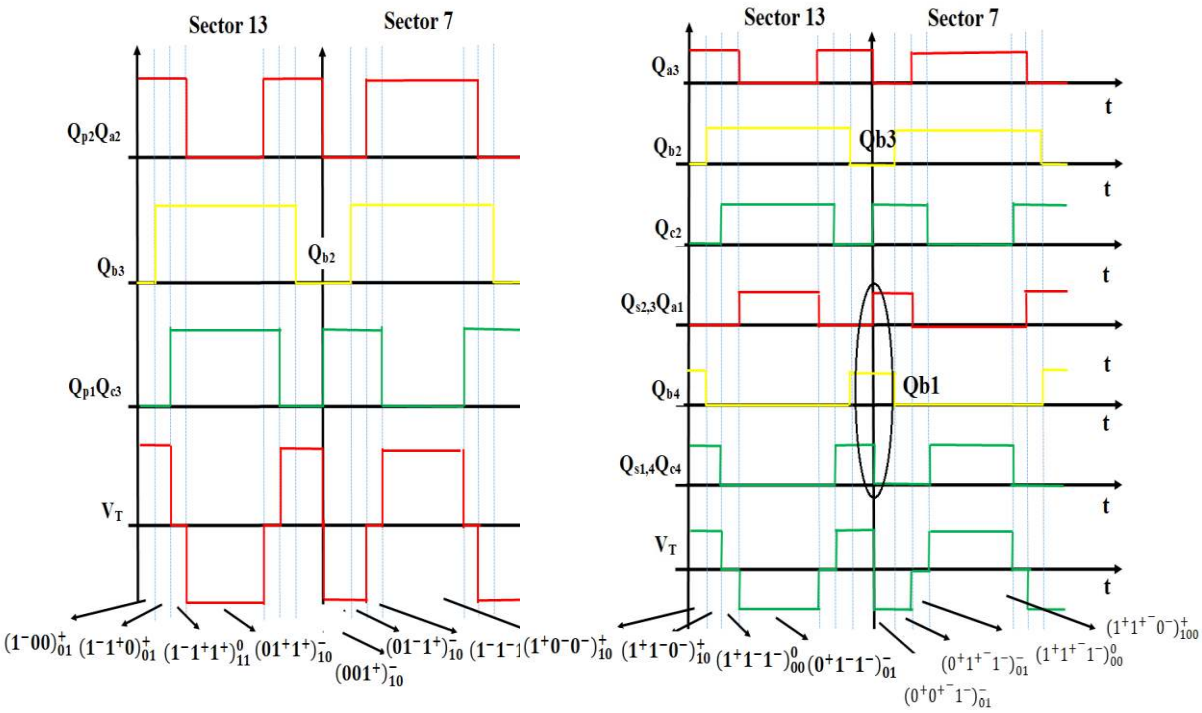

Figure 10. Driving signal of sector 13 and 7 under inverter and rectifier mode.

3.3. Type III:

In this type of SVM, the variations of active and reactive powers of for all the voltage vectors for each sector will be specified and the voltage vector for the sector I is given in the table. 5. Sector I is placed between the angles (θ) -30^0 to 0^0. Furthermore, for the twelve sectors, the angle (θ_n) will be calculated by the following equations:

$$(n-2)\frac{\pi}{6} < \theta_n < (n-1)\frac{\pi}{6} \quad (15)$$

Where, n = 1, 2, 3,.., 12.

Table 5. Active and reactive power variation for sector 1.

$\frac{dp_{inst}}{dt}$		$\frac{dq_{inst}}{dt}$	
>0	<0	>0	<0
$v_0, v_7, v_2, v_3, v_4, v_5$	v_1, v_6	v_0, v_7, v_2, v_3, v_1	v_4, v_5, v_6

Fig.11 consists of six active vectors and two zero vectors, which includes twelve sectors.

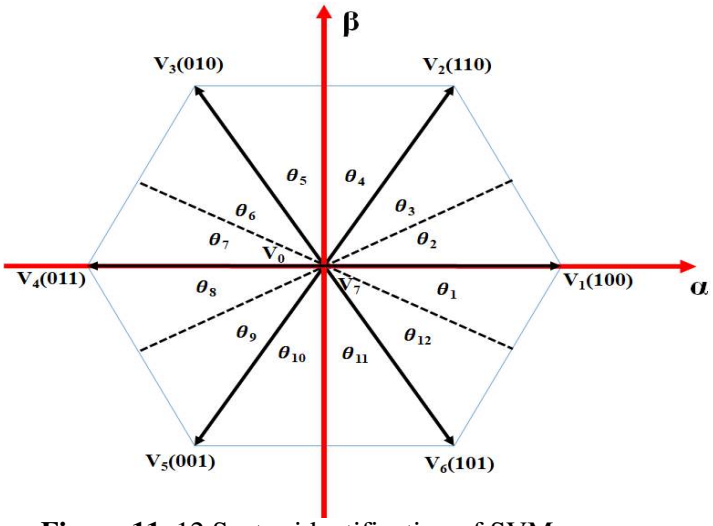

Figure 11. 12 Sector identification of SVM

3.3.1. Power hysteresis comparator

To the active and reactive power for the respective error between instantaneous and its reference value is given by the following equation.

$$\Delta_p = P_{ref} - P_{inst} \; and \; \Delta_q = Q_{ref} - Q_{inst} \tag{16}$$

Hence, the hysteresis comparators are used to digitize the two given vectors. To obtain unity power factor Q_{ref} is set to zero. Fig. 12 shows the active and reactive power for digitized errors.

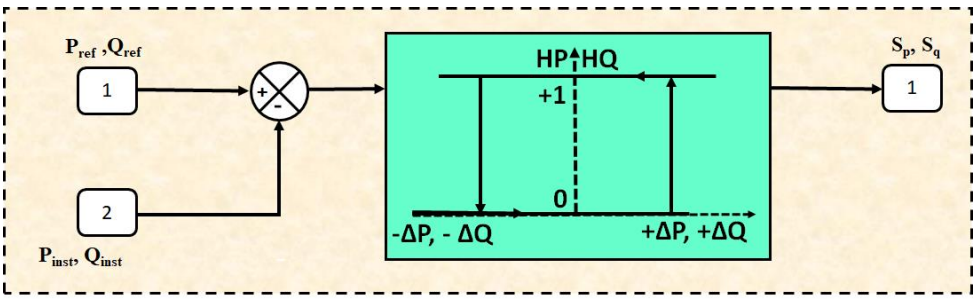

Figure 12. Hysteresis Power Comparator

$$S_p = \begin{cases} 1 \Delta_p > H_p \\ 0 \Delta_p < -H_p \end{cases} \tag{17}$$

$$S_q = \begin{cases} 1 \Delta_q > H_q \\ 0 \Delta_q < -H_q \end{cases} \tag{18}$$

Where H_p and H_q are the hysteresis bands that stipulate the control of active and reactive powers. The input of the hysteresis comparator is injected by the variation Δ_p/Δ_q, to obtain the following cases:

Case I: If the positive hysteresis bands H_p/H_q is less than the variation Δ_p/Δ_q, then the outputs of S_p/S_q, will be equal to 1. Hence, the power is amplified by receiving the driving PWM signals that is applied to the gates of the converter.

Table 6. The new switching table for DPC.

S_p	S_q	θ_1	θ_2	θ_3	θ_4	θ_5	θ_6	θ_7	θ_8	θ_9	θ_{10}	θ_{11}	θ_{12}
1	0	V_5	V_5	V_6	V_6	V_1	V_1	V_2	V_2	V_3	V_3	V_4	V_4
	1	V_0	V_0	V_0	V_0	V_0	V_0	V_0	V_0	V_0	V_0	V_0	V_0
0	0	V_6	V_1	V_1	V_2	V_2	V_3	V_3	V_4	V_4	V_5	V_5	V_6
	1	V_1	V_2	V_2	V_3	V_3	V_4	V_4	V_5	V_5	V_6	V_6	V_1

Case II: If the negative hysteresis bands $-H_p/-H_q$ is greater than the variation Δ_p/Δ_q, then the outputs of S_p/S_q, will be equal to 0. Hence, in this case the power is decreased by receiving the driving PWM signals, which is applied to the gates of the converter.
Case III: If the negative hysteresis bands $-H_p/-H_q$ and the positive hysteresis bands H_p/H_q having the variation Δ_p/Δ_q in between them then the driving PWM signal, which is applied to the gates of the converter follows the previous case.
By using this table 6, the performance of the converter is good with better THD level and by getting a pure sinusoidal form of injected current.
The comparative analysis of different types of Space vector modulation has been given in table 7.

Table 7. Comparison of Different SVM Methods.

	Type – I	**Type – II**	**Type – III**
Switching loss	Decreases	Decreases	Decreases
Conduction loss	Reduced	Reduced	Reduced
DC-link Pole	Contains both balanced and unbalanced dc-link voltages	Contains balanced dc-link voltages	Contains balanced dc-link voltages
Harmonic content	Lower order harmonics are eliminated and reduces output current THD	Reduces output current THD	Reduces output current THD
Additional Elements	Does not require active and passive elements.	Does not require active and passive elements.	Require active and passive elements.

4. Future scope:

Currently, IoT develops widespread in numerous applications, like smart homes, smart city, and smart grid. The IEEE802.11n WLAN is one of the main communication technologies pertinent to IoT applications due to elasticity and low cost, where the well-organized power management is a fundamental necessity of developing IoT applications. In future IoT based smart grids are more popular all over the world. The present scenario shows the smart grid technology and its distribution solutions for the future trend. The IoT plays a vital role in several application domains for control and monitoring of the new security issues, which is taken into an account. The concept of the smart grid is becoming a realism as it progresses from theoretical models to changing stages. Saroj Mondal, and Roy Paily [34] identify a proposed IoT based renewable energies in this smart grid era. The Internet of Things IoT nodes is applied to PV power harvesting system to attain maximum power point tracking (MPPT). Within a tracking error of 0.6%, the IoT tracks the maximum power point in PV system within 12 μs by consuming an intrinsic negative feedback loop. Furthermore, peak pursuing with an efficiency of 99% obtained with rapid changes in atmospheric conditions. By the interaction, sensing, monitoring and control of internal and external environment, the IoT is used. IoT is used to transmit the data by using sensors for

detecting the things, microcontrollers to decrypt the data, and a receiver to connect with the local hub where anyone can make decisions for proper operation of the smart grid. Similarly, the IoT tracks MPP with a tracking error of 0.1% – 0.6%. The IoT application for control and monitoring of BHM is shown in below fig. 13.

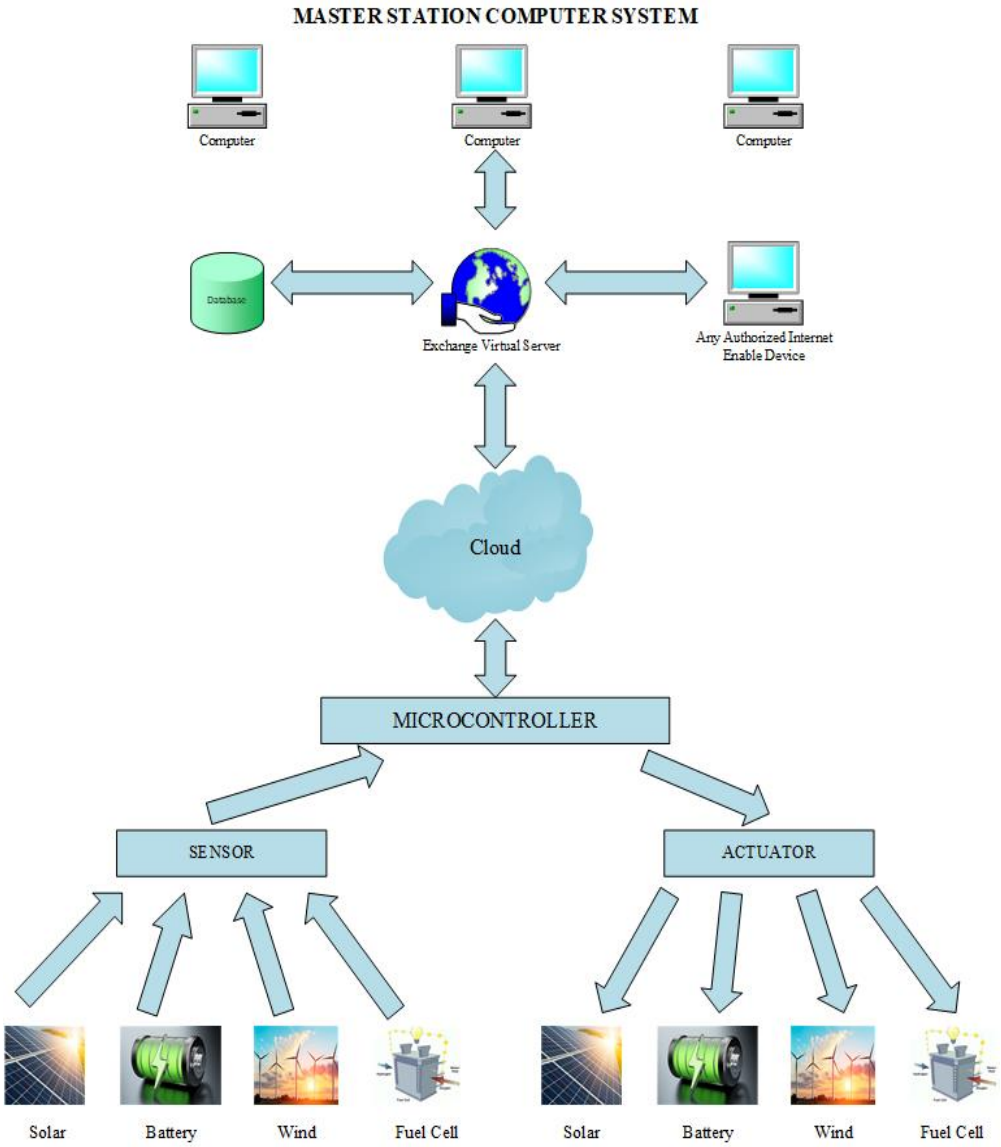

Figure 13. Structural Block diagram of an IoT based Bipolar Hybrid Mirco grid.

5. Conclusion:

A complete review on three-phase bidirectional converter for harmonic elimination has been explored with a detailed perspective on different structures to design and implement this converter for researchers and application engineers. This proposed comparison of this different bidirectional converter and SVM that is provided in this paper is used to easily identify the suitable converter for specified applications. By use of this converter in microgrid there will be a power quality improvement because of higher efficiency, lower cost with a reduced number of switches for the control of voltage and current harmonics, reduced size in a converter, lower cost and reliability in the dc-link voltages. These types of converters produce improved power quality on both ac and dc outputs. The bidirectional AC-DC converter is categorized under two stages namely single and two-stage converter. When compared to two stage converter single stage converter has fewer components, shows more efficiency and low cost,

but it is not popular because of the complex optimization process and control algorithm to maintain the power quality issues. Hence, this paper elaborates on the review of AC/DC bidirectional converter for various applications. One of the new advancements in this microgrid technology is IoT, which is more reliable, controllable and easy to monitor renewable sources.

Reference:

[1] Elizabeth Noghreian, Hamid Reza Koofigar, Power Control of hybrid energy systems with renewable sources (wind-photovoltaic) using switched systems strategy, Sustainable Energy, Grids and Networks 21 (2020) 100280.

[2] C. Yin, H. Wu, F. Locment, M. Sechilariu, Energy management of DC microgrid based on photovoltaic combined with diesel generator and super capacitor, Energy Converters. Manag. 132 (2017) 14–27.

[3] E. Hossain, E. Kabalci, R. Bayindir, R. Perez, Microgrid test beds around the world: State of art, Energy Converters. Manag. 86 (2014) 132–153.

[4] J.Y. Kim, J.H. Jeon, S.K. Kim, C. Cho, J.H. Park, H.M. Kim, K.Y. Nam, Cooperative control strategy of energy storage system and micro sources for stabilizing the microgrid during islanded operation, IEEE Trans. Power Electron. 25 (2010) 3037–3048.

[5] J. Rocabert, G.M.S. Azevedo, A. Luna, J.M. Guerrero, J.I. Candela, P. Rodrguez, Intelligent connection agent for three-phase grid-connected microgrids, IEEE Trans. Power Electron. 26 (2011) 2993–3005.

[6] J. Rocabert, A. Luna, F. Blaabjerg, P. Rodríguez, Control of power converters in AC microgrids, IEEE Trans. Power Electron. 27 (2012) 4734–4749.

[7] Amir Reza Hassani Ahangar, Gevork B. Gharehpetian, Hamid Reza Baghaee, A review on intentional controlled islanding in smart power systems and generalized framework for ICI in microgrids, Electrical Power and Energy Systems 118 (2020) 105709.

[8] Mohsen Eskandari, Li Li, Mohammad. H. Moradi, Improving power sharing in islanded networked microgrids using fuzzy-based consensus control, Sustainable Energy, Grids and Networks 16 (2018) 259–269.

[9] Federico Delfino, Giulio Ferro, Riccardo Minciardi, Michela Robba, Marco Rossi, Mansueto Rossi, "Identification and optimal control of an electrical storage system for microgrids with renewables", Sustainable Energy, Grids and Networks 17 (2019) 100183.

[10] M. Parvez Akter, S. Mekhilef, N. Mei Lin Tan, and H. Akagi, "Modified model predictive control of a bidirectional ac-dc converter based on lyapunov function for energy storage systems," IEEE Transactions on Industrial Electronics, vol. 63, no. 2, pp. 704–715, Feb 2016.

[11] L. H. S. C. Barreto, D. de A. Honrio, D. de Souza Oliveira, and P. P. Praa, "An interleaved-stage acdc modular cascaded multilevel converter as a solution for mv railway applications," IEEE Transactions on Industrial Electronics, vol. 65, no. 4, pp. 3008–3016, April 2018.

[12] K. K. Gupta, A. Ranjan, P. Bhatnagar, L. K. Sahu, and S. Jain, "Multilevel Inverter Topologies With Reduced Device Count: A Review," IEEE Transactions on Power Electronics, vol. 31, no. 1, pp. 135-151, Jan. 2016.

[13] S. Hu, Z. Liang, D. Fan, and X. He, "Hybrid Ultra capacitor-Battery Energy Storage System Based on Quasi-Z-source Topology and Enhanced Frequency Dividing Coordinated Control for EV," IEEE Transactions on Power Electronics, vol. 31, no. 11, pp. 7598-7610, Nov. 2016.

[14] F. Nejabatkhah, Y.W. Li, Overview of power management strategies of hybrid AC/DC microgrid, IEEE Trans. Power Electron. 30 (2015) 7072–7089.

[15] X. Lu, J.M. Guerrero, K. Sun, J.C. Vasquez, R. Teodorescu, L. Huang, Hierarchical control of parallel AC-DC converter interfaces for hybrid microgrids, IEEE Trans. Smart Grid 5 (2014) 683–692.

[16] Ling Gu and Ke Jin," A Three-Phase Bidirectional AC/DC Converter With Y–Δ Connected Transformers", IEEE TRANSACTIONS ON POWER ELECTRONICS, VOL. 31, NO. 12, DECEMBER 2016.

[17] Rohit Baranwal, Kartik V. Iyer, Kaushik Basu, Gysler F. Castelino, and Ned Mohan," A Reduced Switch Count Single-Stage Three-Phase Bidirectional Rectifier With High-Frequency Isolation", IEEE TRANSACTIONS ON POWER ELECTRONICS, VOL. 33, NO. 11, NOVEMBER 2018.

[18] Hammad Armghan, Ming Yang, Ammar Armghan, Naghmash Ali, M.Q. Wang, Iftikhar Ahmad, "Design of integral terminal sliding mode controller for the hybrid AC/DC microgrids involving renewables and energy storage systems", Electrical Power and Energy Systems 119 (2020) 105857.

[19] Farzam Nejabatkhah and Yun Wei Li, "Overview of Power Management Strategies of Hybrid AC/DC Microgrid", IEEE TRANSACTIONS ON POWER ELECTRONICS, VOL. 30, NO. 12, DECEMBER 2015.

[20] Hurng-Liahng Jou, Kuen-Der Wu, Jinn-Chang Wu, You-Zu Lin, Li-Wen Su, "Asymmetric isolated unidirectional multi-level DC-DC power converter", Engineering Science and Technology, an International Journal 22 (2019) 894–898.

[21] S. Hu, Z. Liang, D. Fan, and X. He, "Hybrid ultra capacitor battery energy storage system based on quasi-z-source topology and enhanced frequency dividing coordinated control for ev," IEEE Transactions on Power Electronics, vol. 31, no. 11, pp. 7598–7610, Nov 2016.

[22] Mahmoud A. Sayed , Kazuma Suzuki, Takaharu Takeshita and Wataru Kitagawa," PWM Switching Technique for Three-Phase Bidirectional Grid-Tie DC–AC–AC Converter With High-Frequency Isolation", IEEE TRANSACTIONS ON POWER ELECTRONICS, VOL. 33, NO. 1, JANUARY 2018.

[23] H. Wu, S. Wong, C. K. Tse, and Q. Chen, "Control and modulation of bidirectional single-phase acdc three-phase-leg SPWM converters with active power decoupling and minimal storage capacitance," IEEE Transactions on Power Electronics, vol. 31, no. 6, pp. 4226–4240, June 2016.

[24] P.C. Loh, D. Li, Y.K. Chai, F. Blaabjerg, Autonomous control of interlinking converter with energy storage in hybrid AC-DC microgrid, IEEE Trans. Ind. Appl. 49 (2013) 1374–1382.

[25] Nan Jin, Shiyang Hu , Chun Gan and Zhibin Ling," Finite States Model Predictive Control for Fault-Tolerant Operation of a Three-Phase Bidirectional AC/DC Converter Under Unbalanced Grid Voltages", IEEE TRANSACTIONS ON INDUSTRIAL ELECTRONICS, VOL. 65, NO. 1, JANUARY 2018.

[26] Parviz Najafi, Abbas Hooshmand Viki, Mahdi Shahparasti, " Novel space vector-based control scheme with dc-link voltage balancing capability for 10 switch converter in bipolar hybrid microgrid", Sustainable Energy, Grids and Networks 20 (2019) 100256.

[27] Faouzi Tlili, Ameni Kadri, Faouzi Bacha," Advanced control strategy for bidirectional three phase AC/DC converter", Electric Power Systems Research 179 (2020) 106078.

[28] A. L. Julian and G. Oriti, "A novel clamp circuit for a regenerative rectifier using ac/ac matrix converter theory," IEEE Transactions on Industry Applications, vol. 41, no. 1, pp. 68–74, Jan 2005.

[29] Diogo Varajao, Rui Esteves Araujo, Luis Miguel Miranda and Joao A. Pecas Lopes, "Modulation Strategy for a Single-Stage Bidirectional and Isolated AC–DC Matrix Converter for Energy Storage Systems", IEEE TRANSACTIONS ON INDUSTRIAL ELECTRONICS, VOL. 65, NO. 4, APRIL 2018.

[30] Ling Gu and Ke Jin," A Three-Phase Isolated Bidirectional AC/DC Converter and its Modified SVPWM Algorithm", IEEE TRANSACTIONS ON POWER ELECTRONICS, VOL. 30, NO. 10, OCTOBER 2015.

[31] M. Y. Lee, P. Wheeler, and C. Klumpner, "Space-vector modulated multilevel matrix converter," IEEE Transactions on Industrial Electronics, vol. 57, no. 10, pp. 3385–3394, Oct 2010.

[32] Jonathan E. Bosso, Marcelo Llomplat, Germán Gustavo Oggier, Guillermo Oscar García, "Isolated bidirectional DC-to-three-phase AC converter for integration of renewable energy sources to electric grid", IET Power Electronics, on 28th June 2019.